Infrared Spectra and Density Functional Theory Calculations of Group 6 Transition Metal Sulfides in Solid Argon

Binyong Liang and Lester Andrews*

Department of Chemistry, University of Virginia, P.O. Box 400319, Charlottesville, Virginia 22904-4319

Received: April 10, 2002; In Final Form: May 30, 2002

Laser-ablated chromium, molybdenum, and tungsten atoms react with discharged sulfur vapor during cocondensation in excess argon. On the basis of the metal isotopic splittings, ^{34}S isotopic substitution, and mixed $^{32}S + {}^{34}S$ experiments, the primary reaction product MS_2 molecules are identified. The S−M−S bond angles in the MS_2 molecules are determined from isotopic frequencies as 115° ± 4°, 114° ± 3°, and 114° ± 8° for M = Cr, Mo, and W, respectively. Other reaction products, including CrS, CrS_3, and WS_3, are also characterized. DFT calculations using both B3LYP and BPW91 functionals produce consistent results for the Mo and W compounds and are in excellent agreement with experimental frequencies. For chromium sulfides, the BPW91 functional calculations give satisfactory results.

I. Introduction

Transition metal sulfides are involved in many industrial and biological processes.[1,2] Because of their important roles in biological enzyme systems, catalytic hydrodesulfurization, and solid lubrication, group 6 metal−sulfur cluster compounds, particularly molybdenum sulfides, have been extensively studied.[3−8] In addition, applications are found for molybdenum and tungsten sulfide nanotubes as potential high-performance materials.[9−11] Molecular spectra of transition metal monosulfides are also of special interest to astrophysicists because several lines of TiS and ZrS have been found in the spectra of S-type stars.[12,13]

On the molecular level, group 6 metal sulfides have received comparatively little attention. An earlier thermal emission investigation reported a band system in the region 3860−4650 Å, and an ω''_e value of 621.4 cm^{-1} was deduced for CrS.[14] An argon matrix study reacting transition metal atoms and OCS reported the vibration of CrS at 558 cm^{-1}.[15] A recent high-resolution laser-induced fluorescence spectroscopy study reported the $B^5\Pi_{-1}-X^5\Pi_{-1}$ transition; however, no ω''_e value was given.[16] Two theoretical calculations predicted the $^5\Pi$ ground state for CrS.[16,17] Finally, the D_0 value of CrS^+ was reported in a mass spectroscopic study of the reactions between Cr^+ and CS_2, and OCS.[18] To our knowledge, no study has been reported for higher-order chromium sulfides or for molybdenum and tungsten sulfide molecules. We report here a combined matrix IR and density functional theory investigation of group 6 sulfides.

II. Experimental and Computational Methods

Sulfur atoms and small molecules were generated by a microwave discharge in argon seeded with sulfur vapor. The coaxial quartz discharge tube is similar to the one used in the earlier experiments.[19] Natural isotopic sulfur (Electronic Space Products, Inc., recrystallized) and enriched sulfur (98% ^{34}S, EG&G Mound Applied Technologies) were used as received; different mixtures of the two samples were also employed. The vapor pressure of sulfur located in the sidearm was controlled by the resistively heated windings. The discharge was sustained in the argon−sulfur mixture by an Opthos Instruments 120 W microwave discharge (operated at 30−50% of the maximum power level) with an Evenson−Broida cavity and extended from a region about 5 cm downstream of the sulfur reservoir to the end of the discharge tube. The presence of significant quantities of S_2 in the discharge was indicated by the sky-blue emission,[20,21] different from the normal pink argon discharge.

The experimental method for laser ablation and matrix isolation has been described in detail previously.[22,23] Briefly, the Nd:YAG laser fundamental (1064 nm, 10 Hz repetition rate with 10 ns pulse width, 3−20 mJ/pulse) was focused to ablate the rotating chromium (Johnson-Matthey, 99.2%), molybdenum (Goodfellow), or tungsten (Johnson-Matthey, 99.95%) metal target. Laser-ablated metal atoms were codeposited with a sulfur doped argon stream onto a 7 K CsI cryogenic window at 2−4 mmol/h for 0.5−1.5 h. Infrared spectra were recorded at 0.5 cm^{-1} resolution on a Nicolet 550 spectrometer with 0.1 cm^{-1} accuracy using a mercury cadmium telluride (MCTB) detector down to 400 cm^{-1}. Matrix samples were annealed at different temperatures, and selected samples were subjected to irradiation using a medium-pressure mercury lamp (240−700 nm) with the globe removed.

DFT calculations were performed on all proposed metal sulfides using the Gaussian 98 program[24] and the hybrid B3LYP[25] and pure BPW91[26] functionals. The 6-311+G* basis set was used for sulfur and chromium,[27] and the LanL2DZ effective core potential and basis set were employed for molybdenum and tungsten.[28]

III. Results

Infrared Spectra. Matrix-isolation experiments with laser-ablated metal atoms and discharged sulfur molecules produced common bands in the infrared spectra. These bands[19] include strong absorptions of S_3 at 679.8 and 676.0 cm^{-1}, S_4 at 661.7 and 642.4 cm^{-1}, CS_2 at 1528.0 cm^{-1}, and weak absorption of S_2O at 1157.1 cm^{-1}. The regions that showed new metal-dependent absorption features are presented in Figures 1−6, and the frequencies from various isotopic experiments are listed

10.1021/jp025915+ CCC: $22.00
Published on Web 07/02/2002

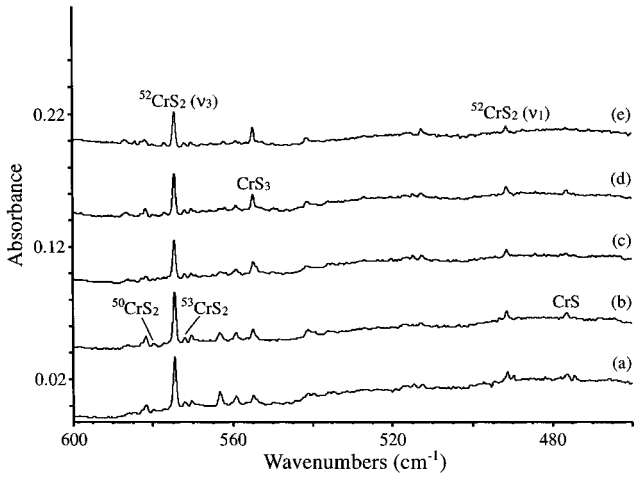

Figure 1. Infrared spectra in the 600−460 cm^{-1} region for laser-ablated Cr codeposited with discharged S in argon at 7 K: (a) sample deposited for 80 min; (b) after 30 K annealing; (c) after λ > 240 nm irradiation; (d) after 35 K annealing; (e) after 40 K annealing.

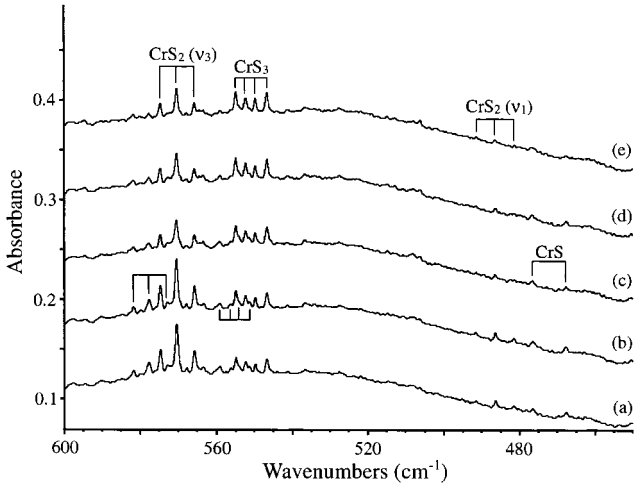

Figure 2. Infrared spectra in the 600−460 cm^{-1} region for laser-ablated Cr codeposited with discharged 50/50 ^{32}S + ^{34}S in argon at 7 K: (a) sample deposited for 40 min; (b) after 30 K annealing; (c) after λ > 240 nm irradiation; (d) after 35 K annealing; (e) after 40 K annealing.

in Table 1. The behaviors of these absorption bands in different experiments and their assignments will be discussed in the next section.

DFT Calculations. As the first step, atomic calculations were performed. The ground electronic state configurations of S, Cr, and Mo atoms were reproduced as [Ne]3s^{2}3p^3, [Ar]3d^{5}4s^1, and [Kr]4d^{5}5s^1. The configuration [Xe]4f^{14}5d^{5}6s^1 is 4.8 and 16.9 kcal/mol lower than the reported W ground-state configuration, [Xe]4f^{14}5d^{4}6s^2, in the B3LYP and BPW91 functional calculations, respectively. The experimental energy separation of these two states is 8.4 kcal/mol.[29] Third-row transition metals are subject to strong relativistic effects and spin−orbit coupling.[30] The current DFT calculations do not include spin−orbit coupling, and the relativistic effect is included through an effective core-potential, that is, quasi-relativistic calculation. Apparently, higher-level calculations that treat these effects specifically are necessary to address the atomic calculation. Nevertheless, this type of calculation has proven effective in characterizing vibrational frequencies of small tungsten-containing molecules.[31,32] Later in this paper, this ^7S state will be treated as the ground state when comparing the relative energies of reactions. Optimized geometries and frequencies were calculated

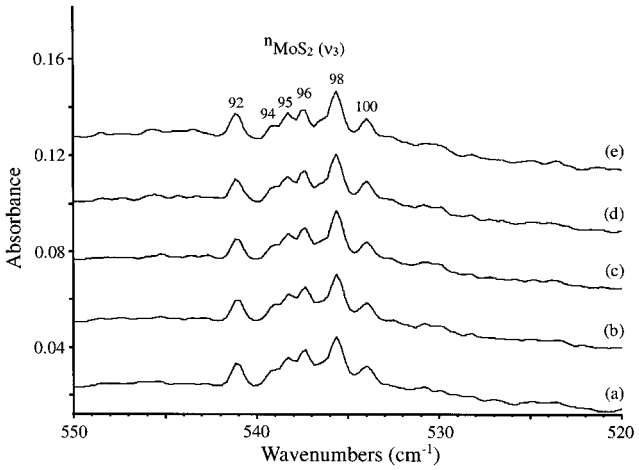

Figure 3. Infrared spectra in the 550−520 cm^{-1} region for laser-ablated Mo codeposited with discharged S in argon at 7 K: (a) sample deposited for 50 min; (b) after 25 K annealing; (c) after 30 K annealing; (d) after 35 K annealing; (e) after 40 K annealing. The numbers on the top of each peak are the mass number of Mo in this MoS_2 vibration (ν_3) absorption.

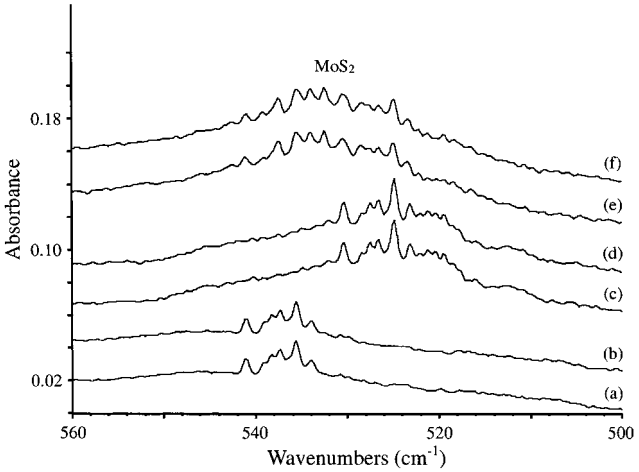

Figure 4. Infrared spectra in the 560−500 cm^{-1} region for laser-ablated Mo codeposited with discharged S in argon at 7 K: (a, b) ^{32}S; (c, d) ^{34}S; (e, f) 50/50 ^{32}S + ^{34}S mixture. Spectra are collected (a, c, e) after deposition or (b, d, f) after 25 K annealing.

for the mono-, di-, and trisulfides of all three metals, and the results are listed in Tables 2−4, respectively. These results will be discussed with the infrared spectra in the next section. For all three metals, the calculated frequencies are listed only for the most abundant metal isotopic components: ^{52}Cr, ^{98}Mo, and ^{184}W.

IV. Discussion

The group 6 transition metal sulfides will be assigned in turn with the help of natural abundance metal and sulfur isotopic substitution and DFT-computed frequencies.

MS_2. *CrS_2.* The reaction between laser-ablated Cr atoms and sulfur produced a strong absorption at 574.6 cm^{-1} (Figure 1). This band showed little change on annealing and decreased by one-third on full-arc irradiation. In the ^{34}S isotopic experiment, this strong band shifted to 565.7 cm^{-1}, with a $^{32}S/^{34}S$ isotopic frequency ratio of 1.0157. In the mixed ^{32}S + ^{34}S experiment (Figure 2), the triplet splitting pattern with relative intensity of 1:2:1 indicates that two equivalent sulfur atoms are involved in this vibrational mode. This band is assigned to the antisymmetric S−Cr−S stretching mode (ν_3) in the CrS_2 molecule. A weaker

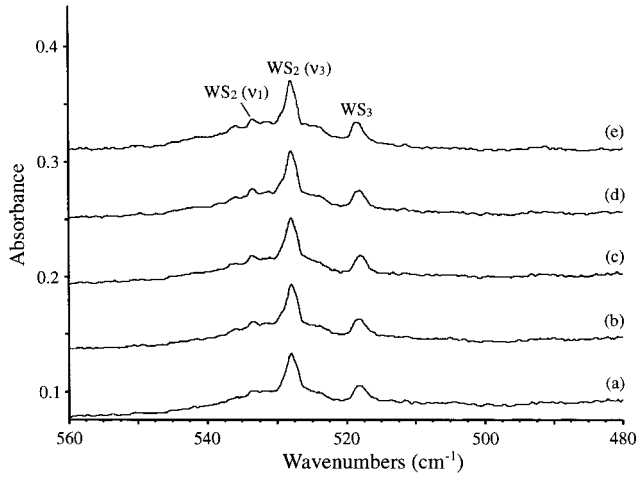

Figure 5. Infrared spectra in the 560−480 cm^{-1} region for laser-ablated W codeposited with discharged S in argon at 7 K: (a) sample deposited for 50 min; (b) after 25 K annealing; (c) after $\lambda > 240$ nm irradiation; (d) after 35 K annealing; (e) after 40 K annealing.

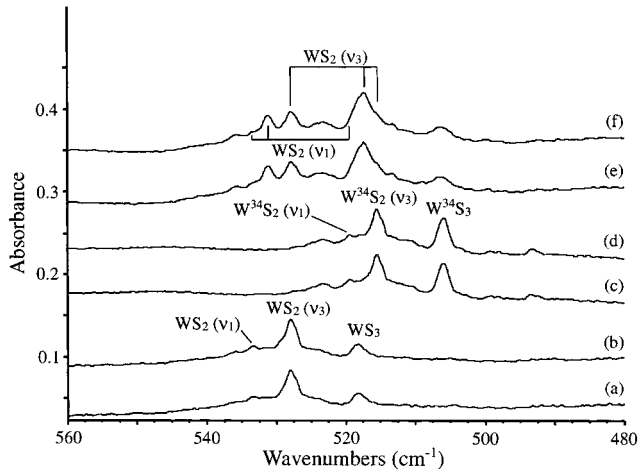

Figure 6. Infrared spectra in the 560−480 cm^{-1} region for laser-ablated W codeposited with discharged S in argon at 7 K: (a, b) ^{32}S; (c, d) ^{34}S; (e, f) 50/50 $^{32}S + {}^{34}S$ mixture. Spectra are collected (a, c, e) after deposition or (b, d, f) after 25 K annealing.

band at 491.3 cm^{-1} tracked with the 574.6 cm^{-1} band throughout the experiment, with only one-fifth of the absorption intensity. This band has the $^{32}S/^{34}S$ isotopic frequency ratio of 1.0204, and again (Figure 2), it showed the triplet splitting pattern in the mixed 50/50 $^{32}S + {}^{34}S$ experiment. This band at 491.3 cm^{-1} is assigned to the symmetric S−Cr−S stretching mode (ν_1) in the same CrS_2 molecule. The association of these two bands at 574.6 and 491.3 cm^{-1} is further confirmed by the fact that their intermediate bands in the mixed $^{32}S + {}^{34}S$ experiments are 0.2 cm^{-1} *higher* and 0.2 cm^{-1} *lower* than the averages of their corresponding pure isotopic bands (Table 1), respectively. For the strong ν_3 mode, two less-abundant metal isotope components, $^{50}CrS_2$ and $^{53}CrS_2$, were observed at 579.9 and 572.1 cm^{-1}, respectively, besides the most dominant ^{52}Cr counterpart at 574.6 cm^{-1}. The relative absorption intensities for these three bands are in accord with the natural-abundance pattern for a single chromium atom (4.35%, 83.79%, and 9.50% for ^{n}Cr, where $n = 50$, 52, and 53, respectively),[33] which confirms that only a single chromium atom is involved in this molecule. The weaker band observed at 581.7 cm^{-1} showed a similar ^{34}S isotopic shift as the 574.6 cm^{-1} band, and split into a 1:2:1 triplet in the mixed $^{32}S + {}^{34}S$ experiment (Figure 2b). This band is assigned to the ν_3 mode of CrS_2 in a different matrix site. Using appropriate G-matrix elements and the Cr and S isotopic ν_3 frequencies,[34,35] we estimated the lower and upper limits for the S−Cr−S bond angle at 111° ± 2° and 119° ± 2°, respectively.

MoS_2. Six bands observed at 541.1, 539.1, 538.3, 537.4, 535.7, and 534.0 cm^{-1} in the Mo sample did not show much change on sample annealing (Figure 3). The relative absorption intensities of these six bands clearly reflect the natural-abundance pattern for a single molybdenum atom, which are

TABLE 1: Infrared Absorptions (cm^{-1}) from Codeposition of Laser-Ablated Cr, Mo, and W Atoms with Discharged Sulfur in Excess Argon

^{32}S	^{34}S	$^{32}S + {}^{34}S$	R(32/34)	identity
		Chromium		
581.7	572.9	581.7, 577.6, 572.9	1.0154	CrS_2 site, ν_3
579.9	571.0		1.0156	$^{50}CrS_2$, ν_3
574.6	565.7	574.6, 570.4, 565.7	1.0157	$^{52}CrS_2$, ν_3
572.1	563.2	572.1, 567.9, 563.2	1.0158	$^{53}CrS_2$, ν_3
570.4	562.1		1.0148	
563.3	555.9		1.0133	
559.3	551.0	559.2, 556.2, 554.0, 551.0	1.0151	CrS_3 site
554.9	546.6	555.0, 552.3, 549.8, 546.7	1.0152	CrS_3
491.3	481.5	491.3, 486.2, 481.5	1.0204	$^{52}CrS_2$, ν_1
476.4	467.7	476.5, 467.7	1.0186	CrS
		Molybdenum		
541.1	530.4		1.0202	$^{92}MoS_2$, ν_3
539.1	528.3		1.0204	$^{94}MoS_2$, ν_3
538.3	527.5		1.0205	$^{95}MoS_2$, ν_3
537.4	526.6		1.0205	$^{96}MoS_2$, ν_3
535.7	524.8		1.0208	$^{98}MoS_2$, ν_3
534.0	523.1		1.0208	$^{100}MoS_2$, ν_3
		Tungsten		
535.9	523.3		1.0241	W_xS_y
533.5	519.4	533.5, 531.3, 519.4	1.0271	WS_2, ν_1
528.0	515.5	528.0, 517.3, 515.5	1.0242	WS_2, ν_3
518.3	505.9	518.3, 513.3, 509.0, 505.9	1.0245	WS_3

TABLE 2: Calculated Electronic State, Relative Energy, Geometry, and Frequencies for MS (M = Cr, Mo, W)

species	electronic state	$\langle S^2\rangle^a$	relative energy [kcal/mol]	geometry [Å]	frequency (intensity) [cm^{-1} (km/mol)]
		B3LYP			
CrS	$^5\Pi$ ($\sigma^1\pi^1\delta^2$)	6.4818 (6.0215)	0	2.125	409.8 (12)
	$^3\Sigma^-$ ($\sigma^2\delta^2$)	2.6754 (2.2862)	+27.8	2.021	472.0 (30)
MoS	$^5\Pi$ ($\sigma^1\pi^1\delta^2$)	6.1526 (6.0020)	0	2.163	466.2 (32)
	$^3\Sigma^-$ ($\sigma^2\delta^2$)	2.4929 (2.0419)	+14.7	2.098	516.9 (72)
WS	$^5\Pi$ ($\sigma^1\pi^1\delta^2$)	6.0690 (6.0006)	0	2.149	496.4 (28)
	$^3\Sigma^-$ ($\sigma^2\delta^2$)	2.0830 (2.0034)	−3.3	2.080	568.3 (12)
		BPW91			
CrS	$^5\Pi$ ($\sigma^1\pi^1\delta^2$)	6.3193 (6.0135)	0	2.085	456.6 (26)
	$^3\Sigma^-$ ($\sigma^2\delta^2$)	2.3210 (2.0588)	+27.3	2.000	530.8 (4)
MoS	$^5\Pi$ ($\sigma^1\pi^1\delta^2$)	6.1118 (6.0014)	0	2.152	486.7 (32)
	$^3\Sigma^-$ ($\sigma^2\delta^2$)	2.0784 (2.0027)	+19.2	2.085	553.0 (35)
WS	$^5\Pi$ ($\sigma^1\pi^1\delta^2$)	6.0769 (6.0008)	0	2.148	493.0 (24)
	$^3\Sigma^-$ ($\sigma^2\delta^2$)	2.0706 (2.0025)	+2.7	2.081	561.9 (6)

[a] Numbers in the parentheses are the $\langle S^2\rangle$ values after annihilation.

TABLE 3: Calculated Electronic State, Relative Energy, Geometry, and Frequencies for MS_2, (M = Cr, Mo, W)

species	electronic state	$\langle S^2\rangle$[a]	relative energy [kcal/mol]	geometry [Å, deg]	frequency (intensity) [cm^{-1}, km/mol] ν_1	ν_2	ν_3
			B3LYP				
CrS_2	$^3B_1$	2.5965 (2.2290)	0	2.054, 121.3	432.1 (2)	133.5 (2)	542.6 (34)
	$^3A_1$	3.3234 (3.0932)	+6.7	2.127, 127.1	365.7 (8)	78.3 (6)	397.1 (3)
	$^1A_1$		+28.3	1.994, 114.0	575.7 (6)	174.2 (0)	619.2 (143)
$Cr(S_2)$	$^5A_2$	6.7309 (6.0195)	+9.2	2.328, 54.2	487.2 (15)	234.4 (2)	175.7 (17)
MoS_2	$^3B_1$	2.0507 (2.0014)	0	2.132, 113.5	523.8 (10)	165.6 (0)	534.8 (118)
	$^3A_1$	2.1599 (2.0105)	+12.4	2.142, 113.4	487.4 (17)	148.3 (1)	503.1 (56)
	$^1A_1$		+14.1	2.113, 107.8	548.3 (12)	185.7 (1)	548.1 (111)
WS_2	$^3B_1$	2.0299 (2.0005)	0	2.132, 113.8	530.1 (8)	161.0 (0)	520.1 (89)
	$^3A_1$	2.0637 (2.0017)	+8.5	2.138, 117.7	517.9 (10)	139.5 (0)	509.3 (63)
	$^1A_1$		+7.0	2.105, 108.3	558.2 (7)	188.4 (0)	543.1 (60)
			BPW91				
CrS_2	$^3B_1$	2.2297 (2.0298)		2.033, 118.0	497.6 (6)	159.4 (0)	574.6 (72)
MoS_2	$^3B_1$	2.0441 (2.0010)		2.135, 112.4	516.4 (9)	170.1 (0)	528.2 (90)
WS_2	$^3B_1$	2.0368 (2.0007)		2.136, 112.8	519.9 (6)	162.8 (0)	513.0 (68)

[a] Numbers in the parentheses are the $\langle S^2\rangle$ values after annihilation.

TABLE 4: Calculated Electronic State, Relative Energy, Geometry, and Frequencies for MS_3, (M = Cr, Mo, W)

species	electronic state	point group	relative energy [kcal/mol]	geometry [Å, deg]	frequency (intensity) [cm^{-1}, km/mol]
			B3LYP		
CrS_3	$^1A_1$	C_3v	0	2.005, 111.8	179.6 (3), 205.2 (2 × 2), 525.5 (2), 603.6 (81 × 2)
	$^1A_1'$	D_3h	+5.6	2.012	154.6i (36), 178.4 (4 × 2), 476.9 (0), 624.4 (78 × 2)
MoS_3	$^1A_1$	C_3v	0	2.138, 107.9	181.5 (1), 192.1 (1 × 2), 521.3 (1), 527.4 (78 × 2)
	$^1A_1'$	D_3h	+15.9	2.147	180.8i (56), 151.8 (2 × 2), 479.0 (0), 546.0 (88 × 2)
WS_3	$^1A_1$	C_3v	0	2.144, 107.7	171.0 (1), 189.5 (0 × 2), 507.8 (59 × 2), 526.6 (0)
	$^1A_1'$	D_3h	+20.5	2.158	199.7i (74), 146.6 (1 × 2), 498.2 (0), 514.2 (73 × 2)
			BPW91		
CrS_3	$^1A_1$	C_3v		2.021, 111.0	190.2 (2), 202.1 (2 × 2), 506.3 (2), 587.1 (65 × 2)
MoS_3	$^1A_1$	C_3v		2.146, 107.1	185.4 (1), 190.9 (1 × 2), 507.7 (1), 518.1 (62 × 2)
WS_3	$^1A_1$	C_3v		2.150, 106.9	174.4 (0), 188.6 (0 × 2), 500.5 (48 × 2), 514.4 (0)

14.84%, 9.25%, 15.92%, 16.68%, 24.13%, and 9.63% for ^{n}Mo, where *n*, the mass number of Mo, equals 92, 94, 95, 96, 98, and 100, respectively.[33] In the ^{34}S experiment (Figure 4c,d), all six molybdenum isotopic counterparts were observed as listed in Table 1. The average of the $^{32}S/^{34}S$ isotopic frequency ratios is 1.0205, which is considerably smaller than the MoS diatomic harmonic frequency ratio of 1.0230. Analogous to CrS_2, these six bands are assigned to the antisymmetric S−^{n}Mo−S stretching mode in the $^n MoS_2$ isotopic molecules. In the $^{32}S + ^{34}S$ experiment (Figure 4e,f), the mixed isotopic bands could not be resolved; however, clearly additional intermediate bands were present. Applying appropriate G-matrix elements and isotopic ν_3 frequencies,[34,35] we estimated the lower and upper limits for the S−Mo−S bond angle at 113° ± 2° and 115° ± 1°, respectively.

WS_2. Similar to the CrS_2 and MoS_2 molecules, the strongest absorption at 528.0 cm^{-1} after sample deposition is assigned to the ν_3 mode of the WS_2 molecule (Figure 5). This band did not show much change on sample annealing and irradiation. In the ^{34}S isotopic experiment (Figure 6c,d), this band red-shifted to 515.5 cm^{-1}, with a $^{32}S/^{34}S$ isotopic frequency ratio of 1.0242. The weaker ν_1 mode in the same molecule was observed at 533.5 cm^{-1} and shifted to 519.4 cm^{-1} in the ^{34}S experiment with an isotopic frequency ratio of 1.0271. The average of the two isotopic frequency ratios equals 1.0257, which is only slightly lower than the WS diatomic harmonic ratio of 1.0260. In the mixed $^{32}S + ^{34}S$ experiment (Figure 6e,f), triplet splitting patterns were observed for both ν_1 and ν_3 modes. The intermediate bands were 4.9 cm^{-1} higher and 4.5 cm^{-1} lower than the medians of their corresponding pure isotopic bands, respectively, showing strong interaction between antisymmetric and symmetric S−W−S stretching modes in this lower symmetry $^{32}S-W-^{34}S$ molecule. Because the heavier apex atom introduces less isotopic separation, the tungsten isotopic splitting pattern could not be resolved in the current experiment, and bands are considerably broader than their analogues in the Cr and Mo experiments. Using sulfur isotopic data for the ν_3 fundamental, we estimated the upper limit of the WS_2 bond angle as 118° ± 5°. On the basis of the WO_2 example,[31] the bond angle is 113° ± 8°.

The chromium group metal atoms all have six valence electrons, and excluding four electrons dedicated to two double bonds with two sulfur atoms, the ground electronic states of metal disulfides are determined by two nonbonding electrons. DFT calculations were first performed with the B3LYP functional for both singlet and triplet spin states, and the ground states are $^3B_1$ for all three metal disulfide molecules. Low-lying excited states are also listed in Table 3, and the singlet $^1A_1$ state becomes more stable with the metal atom changing from Cr to Mo and, finally, to W. Calculations on cyclic metal disulfides were only explored for $Cr(S_2)$, and the lowest state was found as $^5A_2$, which is still 9.2 kcal/mol higher than the $^3B_1$ ground state for CrS_2. The M−S bond lengths in the $^3B_1$ state of MS_2 are 2.054, 2.132, and 2.132 Å, and the S−M−S bond angles are 121.3°, 113.5°, and 113.8° for M = Cr, Mo, and W, respectively. The bond lengths show lanthanide contraction and relativistic effects for tungsten.[30] The S−Mo−S and S−W−S angles are in very good agreement with the experimental results, whereas the calculated S−Cr−S angle is slightly too high. In the vibrational analyses, excellent agreement again is found for MoS_2 and WS_2: the calculated frequencies are within 10 cm^{-1} compared to the argon matrix values. The isotopic frequency

TABLE 5: Comparison of Computed (B3LYP and BPW91) and Experimental Metal−Sulfur Stretching Modes (cm^{-1}) in MS_2 and MS_3

		experimental			B3LYP			BPW91		
species	mode	^{32}S	^{34}S	*R*(32/34)	^{32}S	^{34}S	*R*(32/34)	^{32}S	^{34}S	*R*(32/34)
CrS_2	a_1	491.3	481.5	1.0204	432.1	423.0	1.0215	497.6	487.2	1.0213
	b_2	574.6	565.7	1.0157	542.6	534.3	1.0155	574.6	565.7	1.0157
CrS_3	e	554.9	546.6	1.0152	603.6	594.5	1.0153	587.1	578.2	1.0154
MoS_2	b_2	535.7	524.8	1.0208	534.8	523.9	1.0208	528.2	517.4	1.0209
WS_2	a_1	533.5	519.4	1.0271	530.1	516.0	1.0273	519.9	506.0	1.0275
	b_2	528.0	515.5	1.0242	520.1	507.7	1.0244	513.0	500.7	1.0246
WS_3	e	518.3	505.9	1.0245	507.8	495.7	1.0244	500.5	488.4	1.0248

ratios were calculated at the B3LYP level, as shown in Table 5, and they agree with the observed values. However, for the CrS_2 molecule, the calculated ν_1 and ν_3 vibrational modes are 59.2 and 32.0 cm^{-1} lower than the observed argon matrix values. Comparable calculations were then performed using the BPW91 functional. A different result was obtained for CrS_2, whereas consistent results were found for MoS_2 and WS_2 (Table 3). The S−Cr−S bond angle decreases to 118.0°, which falls between the experimental bond angle limits. The calculated ν_1 and ν_3 vibrational frequencies for CrS_2 are 497.6 and 574.6 cm^{-1}. The exact match for the ν_3 mode is fortuitous, whereas the ν_1 mode is only 6.3 cm^{-1} higher than the argon matrix value.

For unrestricted DFT calculations, $\langle S^2\rangle - S(S+1)$ values are usually cited as measures of "spin contamination", and this "contamination" in fact is a natural part of the unrestricted Kohn−Sham determinant.[36−38] The listed $\langle S^2\rangle$ values in Table 3 clearly show that this problem is encountered for CrS_2. In the B3LYP calculation, the $\langle S^2\rangle$ value for the $^3B_1$ state, 2.5965, deviates greatly from the exact value of 2.0000. The same value after annihilation, which eliminates quintet-state contamination, 2.2290, is still higher than the exact value; this shows that spin states higher than quintet also mix with this $^3B_1$ state. The quintet-state optimization starting with the $^3B_1$ open structure converged to a cyclic $^5A_2$ state, which is only 9.2 kcal/mol higher (Table 3). In the BPW91 calculation, the $\langle S^2\rangle$ value is considerably better than that in the B3LYP calculation: the $\langle S^2\rangle$ value after annihilation, 2.0298, is almost the exact value, which indicates that quintet states are the main source of the contamination in this BPW91 functional calculation. The very different $\langle S^2\rangle$ eigenvalues in the B3LYP and BPW91 functional calculations reveal that the state mixing from higher spin states in the B3LYP calculation mainly comes from the unrestricted Hartree−Fock exchange part, and the results from the pure DFT method (BPW91) are more reliable. As a consequence, the geometry and vibrational frequencies from the BPW91 calculation are in better agreement with the experimental values. Although the restricted open-shell calculation is not recommended,[37] the ROB3LYP calculation on CrS_2 nevertheless was attempted, but this calculation does not converge.

MS_3. *CrS_3.* The band at 554.9 cm^{-1} was weak on deposition (Figure 1a), showed little change on annealing, then increased by a quarter on full-arc irradiation, and sharpened on the following annealing. This band shifted to 546.6 cm^{-1} in the ^{34}S experiment, giving a $^{32}S/^{34}S$ isotopic frequency ratio of 1.0152, which is characteristic of an antisymmetric S−Cr−S stretching mode. Compared to the same frequency ratio of the ν_3 mode (1.0157) in CrS_2, the slightly smaller magnitude for this mode indicates a more acute bond angle. In the mixed 50/50 $^{32}S + ^{34}S$ experiment (Figure 2), this band split into a 2:1:1:2 quartet, which indicates a doubly degenerate mode.[39] Hence, the molecule CrS_3 with either a D_{3h} or a C_{3v} symmetry is identified, and the 554.9 cm^{-1} band is assigned to the doubly degenerate S−Cr−S stretching mode. A nearby band at 559.3 cm^{-1} showed a similar ^{34}S shift and also split into a quartet in the $^{32}S + ^{34}S$ experiment (Figure 2b). The 559.3 cm^{-1} band is assigned to the same mode in CrS_3 at a different matrix site.

WS_3. An analogous tungsten trisulfide was also observed. The band at 518.3 cm^{-1} is assigned to the doubly degenerate S−W−S stretching mode in WS_3. This band shifted to 505.9 cm^{-1} in the ^{34}S experiment, with an appropriate isotopic ratio of 1.0245. Because of several tungsten isotopes, the weaker intermediate bands in the $^{32}S + ^{34}S$ experiment are poorly defined, and only two broad bands were observed with band centers of 513.3 and 509.0 cm^{-1}.

We did not find definitive evidence for MoS_3. In the ^{34}S experiment (Figure 4c,d), several bands were observed just below the $Mo^{34}S_2$ ν_3 absorption, and they are possibly due to the $Mo^{34}S_3$ molecule on the basis of the similar trends in the Cr and W experiments. However, the ^{32}S counterparts of these bands were too weak to be identified, and any possible intermediate components in the mixed isotopic experiments would be covered by isotopic MoS_2 bands.

For six-valence electron chromium group metals, bonding with three sulfur atoms forms closed-shell trisulfides. DFT/B3LYP calculations were first performed on the highest possible D_{3h} symmetry; however, the lowest $^1A_1'$ state in this D_{3h} symmetry for all three metals has one imaginary frequency for bending out of the molecular plane (Table 4). After relaxing the symmetry, both molybdenum and tungsten trisulfides converged in C_{3v} symmetry, and the $^1A_1$ states are 15.9 and 20.5 kcal/mol, respectively, lower than the $^1A_1'$ states in D_{3h} symmetry. More importantly, no imaginary frequency was found. For WS_3, the calculated doubly degenerate stretching mode is predicted at 507.8 cm^{-1}, only 10.5 cm^{-1} lower than the experimental value. Difficult convergence was encountered for the lower-symmetry CrS_3 molecule, and the calculation was finally completed in C_1 symmetry. The converged state possesses essentially a C_{3v} symmetry: bond lengths are different by 0.0001 Å, and bond angles are different no more than 0.005°. This state is denoted as $^1A_1$ in the C_{3v} symmetry, and it is 5.6 kcal/mol more stable than the $^1A_1'$ state. The vibrational analyses produce all real frequencies, and the doubly degenerate stretching mode is predicted at 603.6 cm^{-1}, which is 48.7 cm^{-1} higher than the argon matrix value. Calculations using the BPW91 functional give comparable results (Table 4). Isotopic frequency ratios are listed in Table 5, which are in excellent agreement with the observed values.

MS. *CrS.* The weak band observed at 476.4 cm^{-1} on deposition (Figure 1a) increased slightly on annealing to 25 K, then decreased on the ultraviolet irradiation and annealing to 40 K. In the ^{34}S isotopic experiment, this band shifted to 467.7 cm^{-1}, with a $^{32}S/^{34}S$ isotopic frequency ratio of 1.0186. In the mixed $^{32}S + ^{34}S$ experiment, only a doublet with two pure isotopic bands was observed (Figure 2), which indicates that only one sulfur atom is involved in this vibrational mode. The isotopic ratio of 1.0186 is only slightly lower than the diatomic

TABLE 6: Relative Energies (kcal/mol) of the Reactions in the DFT Calculations with ZPE Corrections

reactions	M = Cr[a]	M = Mo[a]	M = W[a]
(1) M (^{7}S) + S (^{3}P) → MS ($^5\Pi$)	−69.9 (−76.7)	−79.0 (−85.7)	−99.1 (−101.5)
(2) M (^{7}S) + S_2 ($^3\Sigma_g^-$) → MS ($^5\Pi$) + S (^{3}P)	23.2 (25.4)	14.1 (16.3)	−6.0 (0.5)
(3) M (^{7}S) + S_3 ($^1A_1$) → MS ($^5\Pi$) + S_2 ($^3\Sigma_g^-$)	−25.1 (−20.7)	−34.2 (−29.7)	−54.3 (−45.6)
(4) M (^{7}S) + S_2 ($^3\Sigma_g^-$) → MS_2 ($^3B_1$)	−49.0 (−65.2)	−81.8 (−91.4)	−121.1 (−122.2)
(5) M (^{7}S) + S_3 ($^1A_1$) → MS_2 ($^3B_1$) + S (^{3}P)	−4.2 (−9.3)	−37.0 (−35.5)	−76.3 (−66.2)
(6) M (^{7}S) + S_3 ($^1A_1$) → MS_3 ($^1A_1$)	−54.4 (−86.1)	−121.4 (−133.7)	−175.5 (−176.3)
(7) MS ($^5\Pi$) + S_2 ($^3\Sigma_g^-$) → MS_3 ($^1A_1$)	−29.2 (−65.5)	−87.2 (−104.0)	−121.2 (−130.7)
(8) MS_2 ($^3B_1$) + S (^{3}P) → MS_3 ($^1A_1$)	−50.2 (−76.9)	−84.4 (−98.2)	−99.2 (−110.1)
(9) MS_2 ($^3B_1$) + S_3 ($^1A_1$) → MS_3 ($^1A_1$) + S_2 ($^3\Sigma_g^-$)	−5.4 (−20.9)	−39.6 (−42.3)	−54.5 (−54.1)

[a] Numbers without parentheses are calculated using the B3LYP functional, and numbers in parentheses are calculated using the BPW91 functional.

$Cr^{32}S/Cr^{34}S$ harmonic frequency ratio of 1.0189. This band is assigned to the CrS fundamental in the argon matrix. In the current experiments, no evidence was found for MoS and WS, which could be due to weak oscillator strengths for the heavier metal monosulfides.

A gas-phase electronic emission spectroscopic study reported the ω''_e value 621.4 cm^{-1} for CrS in a King's furnace at about 2200 °C;[14] however, it has been questioned whether the band system involved the ground state.[16] In an earlier argon matrix infrared study using OCS as the sulfur source, the authors assigned a band at 558 cm^{-1} to the stretching frequency of CrS without support from the isotopic substitution.[15] Two theoretical calculations on CrS predicted the ground state as $^5\Pi$ ($\sigma^1\pi^1\delta^2$), and the ω''_e values vary from 517 to 418 cm^{-1} using different methods.[16,17] Apparently, the two earlier experimental values for the CrS vibration are too high.

Our DFT calculation on CrS reproduced the $^5\Pi$ ground state, whereas the $^3\Sigma^-$ ($\sigma^2\delta^2$) state is 27.8 and 27.3 kcal/mol higher in the B3LYP and BPW91 functional calculations, respectively. Spin contamination is also present in CrS, and the B3LYP functional calculation shows a greater degree of mixing with higher spin states. The calculated harmonic frequency is 409.8 and 456.6 cm^{-1} using B3LYP and BPW91, respectively, which is lower than the 476.4 cm^{-1} argon matrix frequency. Similar to the case in CrS_2, better agreement is found for the BPW91 functional calculation because of less "spin contamination".

The bonding in transition metal monosulfides has been discussed in earlier work.[17,40] For earlier transition metals, the bonding has triple-bond character, which includes the σ bond between metal hybridized dsσ and sulfur 3pσ orbital electrons and the π bonds between metal dπ and sulfur pπ orbital electrons. The bonding changes to a double bond for chromium, because the metal dπ orbitals start to be filled, which eliminates the π-back-donation from sulfur. In $^5\Pi$ ground-state CrS, orbitals involved in the valence configuration $\sigma^1\pi^1\delta^2$ are mainly chromium atomic orbitals: the σ orbital is mainly the Cr 4s orbital, whereas both π and δ orbitals are derived from 3d orbitals. When the metal atoms in monosulfides change from Cr to Mo and W, the relativistic effect[30] makes the s orbital more compact and stable compared to the d orbitals; hence, the $^3\Sigma^-$ ($\sigma^2\delta^2$) states become more stable (Table 2). In tungsten monosulfide, the $^5\Pi$ and $^3\Sigma^-$ states almost possess the same energies, and different energy orders are predicted for B3LYP and BPW91 functional calculations. Detailed experimental study and high-level calculations are necessary to determine the ground state for WS.

Other Absorptions. In the chromium experiment, weak bands at 570.4 and 563.3 cm^{-1} remain unassigned. The 570.4 cm^{-1} band is close to the ν_3 vibration of CrS_2; however, the $^{32}S/^{34}S$ isotopic frequency ratio is lower, and the isotopic splitting pattern is covered by other stronger bands in the mixed isotopic experiment. The 563.3 cm^{-1} band decreased on annealing and disappeared on full-arc irradiation. The band has a very low $^{32}S/^{34}S$ isotopic frequency ratio of 1.0133, but the splitting pattern in the mixed isotopic experiment is not resolved. It is possible that this absorption is due to an anionic species, but insufficient evidence is available for definitive assignment.

In the tungsten experiment, a weak band at 535.9 cm^{-1} only differs from the ν_3 mode of WS_2 by 7.9 cm^{-1}, and the $^{32}S/^{34}S$ isotopic ratio of 1.0242 indicates an antisymmetric S−W−S stretching mode. It may be assigned to the ν_3 mode of WS_2 at another matrix site; however, the isotopic splitting pattern could not be resolved in the mixed isotopic experiment. This band increased slightly on annealing, which indicates it could be a higher-order complex. We only generically assign it as W_xS_y.

Thermochemistry. Possible reactions for product formation, along with zero-point-energy (ZPE)-corrected relative energy changes calculated by DFT are listed in Table 6. The ΔE values for reaction 1 are actually $-D_0$ values for the MS molecules. Only D_0 for CrS has been measured experimentally as 3.37 eV (77.7 kcal/mol),[41] and our calculated values, especially the BPW91 functional calculated value of 76.7 kcal/mol, agree with the experimental value. Two different DFT calculations produced comparable ΔE values for molybdenum and tungsten reactions, whereas large discrepancy was found for the reactions forming CrS_2 and CrS_3. Because the BPW91 functional calculations produce $\langle S^2 \rangle$ values closer to exact values in open-shell systems and also generate vibrational frequencies in better agreement with our experimental values, the ΔE values in the BPW91 calculations are more reliable for Cr systems.

Reaction mechanisms forming MS and MS_2 cannot be determined in the current experiments. All reactions, except reaction 2, are exothermic on the basis of the DFT calculations; however the reactions forming MS and MS_2 apparently require significant activation energies because the infrared absorptions of MS and MS_2 do not increase upon annealing and irradiation. During the laser-deposition processes, reactions 1−6 all can happen because laser-ablated metal atoms provide sufficient excess energies to overcome the reaction barriers.[42] Reactions 2 and 4 are probably more important because S_2 is expected to be the major sulfur reagent, although its concentration could not be measured, and MS_2 is the dominant product.

Significant MS_3 products were observed upon deposition for both Cr and W experiments. Direct reactions between M and S_3 probably form initial adducts, which are quenched and rearrange in the argon matrix to give MS_3. Reactions 7−9 probably occur in the irradiation process for chromium because the CrS_3 absorption increases while both the CrS and CrS_2 absorptions decrease (Figures 1c and 2c).

V. Conclusions

Laser-ablated chromium, molybdenum, and tungsten metal atoms react with discharged sulfur vapor during cocondensation

in excess argon. For all three metals, the primary reaction MS_2 products are identified through isotopic substitution and mixed isotopic experiments. The ν_1 and ν_3 modes are observed at 491.3 and 574.6 cm^{-1} for CrS_2 and 533.5 and 528.0 cm^{-1} for WS_2, while only the ν_3 mode is observed for MoS_2 at 535.7 cm^{-1}. Using resolved metal isotopic absorptions for CrS_2 and MoS_2 and sulfur isotopic absorptions for the antisymmetric stretching mode, we determined the S−M−S bond angles as 115° ± 4°, 114° ± 3°, and 114° ± 8° for M = Cr, Mo, and W, respectively. Other metal sulfides are also identified: the CrS fundamental absorbs at 476.4 cm^{-1}, and the doubly degenerate M−S bond stretching modes absorb at 554.9 and 518.3 cm^{-1} for CrS_3 and WS_3, respectively.

The group 6 metal sulfides are analogous to the group 6 metal oxides investigated previously.[31,43,44] The dominant products are the metal disulfides and metal dioxides, and evidence is found for trisulfides and trioxides.

Both pure and hybrid DFT calculations have been performed on product molecules. For molybdenum and tungsten sulfides, both methods produced consistent results, which are in excellent agreement with the experimental values. For chromium sulfides, spin contamination is significant for the hybrid B3LYP functional calculations, whereas the pure BPW91 functional calculations produced satisfactory results and are in good agreement with the experimental values.

Acknowledgment. The authors gratefully acknowledge National Science Foundation support from Grant CHE 00-78836 and helpful discussions with C. W. Bauschlicher, Jr., and C. O. Trindle.

References and Notes

(1) Stiefel, E. I., Matsumoto, K., Eds. *Transition Metal Sulfur Chemistry, Biological and Industrial Significance*; American Chemical Society: Washington, DC, 1997.

(2) Weber, T., Prins, R., van Santen, R. A., Eds. *Transition Metal Sulphides, Chemistry and Catalysis*; NATO ASI Series; Kluwer Academic Publishers: Dordrecht, Netherlands, 1998.

(3) Stiefel, E. I. *Pure Appl. Chem.* **1998**, *70*, 889.

(4) Heising, J.; Kanatzidis, M. G. *J. Am. Chem. Soc.* **1999**, *121*, 638.

(5) Heising, J.; Kanatzidis, M. G. *J. Am. Chem. Soc.* **1999**, *121*, 11720.

(6) Wu, L. M.; Zhang, Y. F.; Hu, J. M.; Zhou, L. X.; Li, J. Q. *J. Mol. Struct. (THEOCHEM)* **1999**, *460*, 27.

(7) Zakharov, I. I.; Startsev, A. N. *J. Phys. Chem. B* **2000**, *104*, 9025.

(8) Bezverkhy, I.; Afanasiev, P.; Lacroix, M. *Inorg. Chem.* **2000**, *39*, 5416.

(9) Chhowalla, M.; Amaratunga, G. A. J. *Nature*, **2000**, *407*, 164.

(10) Remskar, M.; Mrzel, A.; Skraba, Z.; Jesih, A.; Ceh, M.; Demšar, J.; Stadelmann, P.; Lévy, F.; Mihailovic, D. *Science*, **2001**, *292*, 479.

(11) Nath, M.; Mukhopadhyay, K.; Rao, C. N. R. *Chem. Phys. Lett.* **2002**, *352*, 163.

(12) Jonsson, J.; Launila, O.; Lindgren, B. *Mon. Not. R. Astron. Soc.* **1992**, *258*, 49.

(13) Lambert, D. L.; Clegg, R. E. S. *Mon. Not. R. Astron. Soc.* **1980**, *191*, 367.

(14) Monjazeb, A.; Mohan, H. *Spectrosc. Lett.* **1973**, *6*, 143.

(15) DeVore, T. C.; Franzen, H. F. *High Temp. Sci.* **1975**, *7*, 220.

(16) Shi, Q.; Ran, Q.; Tam, W. S.; Leung, J. W.-H.; Cheung, A. S.-C. *Chem. Phys. Lett.* **2001**, *339*, 154.

(17) Bauschlicher, C. W., Jr.; Maitre, P. *Theor. Chim. Acta* **1995**, *90*, 189.

(18) Rue, C.; Armentrout, P. B.; Kretzschmar, I.; Schroder, D.; Schwarz, H. *Int. J. Mass Spectrom.* **2001**, *210/211*, 283.

(19) Brabson, G. D.; Mielke, Z.; Andrews, L. *J. Phys. Chem.* **1991**, *95*, 79.

(20) Long, S. R.; Pimentel, G. C. *J. Chem. Phys.* **1977**, *66*, 2219.

(21) Smardzewski, R. R. *J. Chem. Phys.* **1978**, *68*, 2878.

(22) Burkholder, T. R.; Andrews, L. *J. Chem. Phys.* **1991**, *95*, 8697.

(23) Hassanzadeh, P.; Andrews, L. *J. Phys. Chem.* **1992**, *96*, 9177.

(24) Frisch, M. J.; Trucks, G. W.; Schlegel, H. B.; Scuseria, G. E.; Robb, M. A.; Cheeseman, J. R.; Zakrzewski, V. G.; Montgomery, J. A., Jr.; Stratmann, R. E.; Burant, J. C.; Dapprich, S.; Millam, J. M.; Daniels, A. D.; Kudin, K. N.; Strain, M. C.; Farkas, O.; Tomasi, J.; Barone, V.; Cossi, M.; Cammi, R.; Mennucci, B.; Pomelli, C.; Adamo, C.; Clifford, S.; Ochterski, J.; Petersson, G. A.; Ayala, P. Y.; Cui, Q.; Morokuma, K.; Malick, D. K.; Rabuck, A. D.; Raghavachari, K.; Foresman, J. B.; Cioslowski, J.; Ortiz, J. V.; Stefanov, B. B.; Liu, G.; Liashenko, A.; Piskorz, P.; Komaromi, I.; Gomperts, R.; Martin, R. L.; Fox, D. J.; Keith, T.; Al-Laham, M. A.; Peng, C. Y.; Nanayakkara, A.; Gonzalez, C.; Challacombe, M.; Gill, P. M. W.; Johnson, B. G.; Chen, W.; Wong, M. W.; Andres, J. L.; Head-Gordon, M.; Replogle, E. S.; Pople, J. A. *Gaussian 98*, revision A.1; Gaussian, Inc.: Pittsburgh, PA, 1998.

(25) Lee, C.; Yang, E.; Parr, R. G. *Phys. Rev. B* **1988**, *37*, 785.

(26) Perdew, J. P.; Wang, Y. *Phys. Rev. B* **1992**, *45*, 13244.

(27) McLean, A. D.; Chandler, G. S. *J. Chem. Phys.* **1980**, *72*, 5639. Wachters, A. J. H. *J. Chem. Phys.* **1970**, *52*, 1033. Hay, P. J. *J. Chem. Phys.* **1977**, *66*, 4377. Raghavachari, K.; Trucks, G. W. *J. Chem. Phys.* **1989**, *91*, 1062.

(28) Hay, P. J.; Wadt, W. R. *J. Chem. Phys.* **1985**, *82*, 270. Wadt, W. R.; Hay, P. J. *J. Chem. Phys.* **1985**, *82*, 284. Hay, P. J.; Wadt, W. R. *J. Chem. Phys.* **1985**, *82*, 299.

(29) Moore, C. E. *Atomic Energy Levels*; National Bureau of Standards (U.S.) Circular 467; National Bureau of Standards: Washington, DC, 1958.

(30) Pyykkö, P. *Chem. Rev.* **1988**, *88*, 563.

(31) Zhou, M. F.; Andrews, L. *J. Chem. Phys.* **1999**, *111*, 4230 (W + O_2).

(32) Wang, X.; Andrews, L. *J. Am. Chem. Soc.* **2002**, *124*, 5636 (WH_6).

(33) *CRC Handbook of Chemistry and Physics*; CRC Press: Boca Raton, FL, 1985.

(34) Allavena, M.; Rysnik, R.; White, D.; Calder, V.; Mann, D. E. *J. Chem. Phys.* **1969**, *50*, 3399.

(35) Andrews, L. *J. Electron Spectrosc. Relat. Phenom.* **1998**, *97*, 63.

(36) Wang, J.; Becke, A. D.; Smith, V. H., Jr. *J. Chem. Phys.* **1995**, *102*, 3477.

(37) Pople, J. A.; Gill, P. M. W.; Handy, N. C. *Int. J. Quantum Chem.* **1995**, *56*, 03.

(38) Grafenstein, J.; Cremer, D. *Mol. Phys.* **2001**, *99*, 981.

(39) Darling, J. H.; Ogden, J. S. *J. Chem. Soc., Dalton Trans.* **1972**, 2496.

(40) Liang, B.; Andrews, L. *J. Phys. Chem. A* **2002**, *106*, 3738; *J. Phys. Chem. A* **2002**, *106*, 6295.

(41) Huber, K. P.; Herzberg, G. *Constants of Diatomic Molecules*; Van Nostrand Reinhold: New York, 1979.

(42) Kang, H.; Beauchamp, J. L. *J. Phys. Chem.* **1985**, *89*, 3364.

(43) Chertihin, G. V.; Bare, W. D.; Andrews, L. *J. Chem. Phys.* **1997**, *107*, 2798.

(44) Bare, W. D.; Souter, P. F.; Andrews, L. *J. Phys. Chem. A* **1998**, *102*, 8279.